International Journal of Technology

http://ijtech.eng.ui.ac.id



Research Article

Facile and Sustainable Arc Plasma-Assisted Synthesis of Mesoporous Carbon: Characterization and Application as a CO₂ Adsorbent

Ary Mauliva Hada Putri ^{1,2}, Rakhael Cahya Nugraheni Budiharja ¹, Benni F. Ramadhoni ^{1,2}, Yuliusman ¹, Yuswan Muharam ^{1,*}

Abstract: Increasing CO₂ concentrations in the atmosphere have an impact on rising temperatures and climate change. CO₂ separation through the adsorption process is an attractive option due to its low energy consumption and installation costs. Activated carbon was chosen as the adsorbent because it has a better CO₂ adsorption capacity at atmospheric pressure and high temperature. Tea twigs can be used as a raw material for activated carbon because of their high carbon content (53%). This research was conducted to produce activated carbon through carbonization at 400°C for 1 h using a flow of N₂, followed by physical activation using arc plasma, which can generate high heat in a short time compared to electric furnace. Activation temperature variations from 600°C to 800°C were applied in this study to observe their effects on the characteristics of the activated carbon produced. Characterization analysis, including surface area, functional group formation, and crystal structure and size, was conducted using Brunauer-Emmett-Teller (BET), Fourier transform infrared (FTIR), and X-ray diffraction (XRD) analyses, respectively. Morphological changes in the activated carbon from plasma activation were analyzed using a scanning electron microscope (SEM). The performance of the activated carbon in adsorbing CO₂ was measured using Temperature-Programed Desorption of CO₂ (TPD-CO₂ at a temperature of 40°C and a pressure of 1 atm. The optimum surface area obtained in this study was 86.668 m² g⁻¹ with an adsorption capacity of 2.057 mmol g⁻¹, which was achieved using Arc Plasma at a physical activation temperature of 700°C with an activation time of 4 min.

Keywords: Activated carbon; Adsorption; Arc plasma; Carbon dioxide; Tea twigs

1. Introduction

According to data from the International Energy Agency (Agency, 2023), CO₂ concentrations in the atmosphere are increasing by 1% annually. This condition has several environmental impacts, including climate change and rising surface temperatures. The burning of fossil fuels in various industries, such as power generation, contributes to CO₂ emissions in the atmosphere. Therefore, efforts are needed to reduce the amount of CO₂ emissions through various mitigation measures, including separating CO₂ from industrial waste gases using CO₂ separation methods.

This work was supported by the Ministry of Education, Culture, Research, and Technology of the Republic of Indonesia funded by the Operational Assistance Program for State Universities – Doctoral Dissertation Research Program (Fiscal Year 2024), number: NKB-975/UN2.RST/HKP.05.00/2024 and 350/PKS/WR III/UI/2024.

 $^{^{1}}$ Department of Chemical Engineering, Universitas Indonesia, Depok, West Java, 16425, Indonesia

²Research Center for Chemistry-National Research and Innovation Agency, Building 452, Kawasan Sains dan Teknologi BJ Habibie, PUSPIPTEK, Serpong, South Tangerang, 15314, Indonesia

^{*}Corresponding author: muharam@che.ui.ac.id, Tel.: 62-21-7863516

Current technologies for separating CO₂ from waste gases include absorption, adsorption, membranes, and cryogenic distillation. Adsorption has gained considerable attention among these technologies and can serve as an alternative strategy for CO₂ separation from waste gases. The advantages of the adsorption process include high absorption capacity, good selectivity, efficient regeneration, favorable adsorption and desorption kinetics, excellent chemical stability, and low energy consumption (Gomez-Delgado et al., 2022; Guo et al., 2021; Gundogdu et al., 2012).

The CO₂ separation in this study focuses on the post-combustion waste gas condition, where the CO₂ concentration ranges from 3% to 20% (Lai et al., 2021). Several types of solid adsorbents, including zeolites, metal organic frameworks (MOFs), and activated carbon, are used in the adsorption process. Activated carbon demonstrates superior CO₂ adsorption capacity at a pressure of 1 bar and a temperature of 40-60°C, which aligns with the operational conditions of post-combustion CO₂ (Lai and Ngu, 2024). In contrast to zeolites, which are hydrophilic, activated carbon exhibits hydrophobic properties and is insoluble in water (Lai et al., 2021; Karamah et al., 2019).

Activated carbon (AC) can be produced from various materials with high C content. Other criteria needed for activated carbon production include low inorganic content, such as low ash content, minimal degradation during storage, and abundant availability in nature. Activated carbon derived from biomass waste, including coconut shells (49.62%) (Iqbaldin et al., 2013), tea grounds (48,70%) (Zhou et al., 2018), bagasse (Han et al., 2019), palm kernel shell (51%) (Yek et al., 2019), and rice husk (36.52%) (Boonpoke et al., 2010), has been extensively studied.

Tea twigs were selected as the adsorbent material in this study due to their high carbon content (53.28%), low ash content (1.69%), volatile matter content (76.59%), and high lignin content (39.5%). The high lignin content in the biomass can facilitate the formation of micropores in the carbonized biochar (Eliasson and Carlsson, 2020; Panahi et al., 2020; Tabak et al., 2019). In 2021, tea production in Indonesia reached 137,800 tons (BPS, 2023). The amount of waste generated from tea processing in factories accounts for 3% of the total tea production, or 4,134 tons per year (Wulansari and Rezamela, 2020). Tea twigs can account for up to 77% of the total tea waste (Rosyadi, 2018). The actantial waste from tea twigs in Indonesia amounts to 3,183 tons per year.

The production of activated carbon involves two stages: carbonization and activation. Activation is divided into chemical and physical activation. Physical activation is an environmentally friendly method as it does not use chemicals. Generally, physical activation is performed at high temperatures of around 500-800°C with a slow heating rate using steam, CO₂, or air. González-Garca et al. (2013) utilized activation temperatures of 750-800°C, yielding activated carbon with a surface area of 822-1,333 m² g⁻¹ and a CO₂ adsorption capacity of 1.6-1.9 mmol g⁻¹ (González-García et al., 2013). However, activation temperatures above 850°C can damage the porosity and reduce the surface area. This indicates that the activation temperature has a significant impact on the activated carbon's surface area and adsorption capacity.

Although physical activation is an environmentally friendly activation method that is free from chemicals, it has a longer processing time, ranging from 1 to 8 hours (Heidarinejad et al., 2020); (Luo, 2020); (Plaza-Recobert et al., 2017); (González-García et al., 2013). Kuptajit et al. (2021) studied the use of thermal plasma in the production of activated carbon through microwave plasma.(Kuptajit et al., 2021) The results of the study demonstrated that microwave plasma heating produces activated carbon with a surface area of 11-1,007 m² g⁻¹ for 2 min. Therefore, the use of thermal plasma to produce activated carbon has actantial for further research and development.

Arc plasma is a device that generates thermal plasma through the ionization of gas between the actantial difference of the anode and cathode with a pulsed current. The Arc Plasma device does not have a temperature control, but it controls the electric current. In the Arc Plasma, a torch is used as the site where electrical discharge occurs due to the actantial difference between the cathode and anode. The argon gas is directed into the torch, which is equipped with a cooling water system. In addition to acting as a plasma-forming gas, argon protects the material from oxidation. During arc discharge, the cathode temperature is extremely high, and thermal electrons are emitted from the cathode. The light emitted from the plasma often contains lines originating from the cathode

material. Adjusting the pulsed electric current controls the heat generated by the arc plasma, with the current serving as the input source for heat generation. During operation, the temperature generated ranges between 600-2000°C, with a shorter heating time compared to the electric furnace. The heat produced by the arc plasma can be measured using a thermocouple. The thermocouple temperature readings serve as the control parameter in the physical activation process. Arc plasma sintering has the advantages of high energy density, low voltage, and high current. Currently, Arc plasma has not been applied to activated carbon.

No prior research has been conducted on the synthesis of activated carbon through physical activation using arc plasma. Activation with Arc Plasma presents several benefits, including a shorter activation time compared to electric furnaces. In this study, activated carbon was synthesized through physical activation using Arc Plasma, and the pore surface characteristics of the activated carbon were obtained through characterization tests. The resulting activated carbon from this study was used for CO₂ adsorption using Temperature-Programed Desorption of CO₂ (TPD-CO₂ at a pressure of 1 bar and a temperature of 40°C. Brunauer-Emmett-Teller (BET) and scanning electron microscopy (SEM) characterization were also performed to determine the surface area of the activated carbon and to observe changes in the morphology or pore structure of the raw material and the produced activated carbon. Fourier transform infrared (FTIR) and X-ray diffraction (XRD) were conducted to obtain information about the functional groups present in the activated carbon, as well as the structure and crystal size of the samples.

2. Methods

2.1. Raw Materials

Tea twigs that are not used in the tea production process were used as the main material in this study. The tea twigs were washed and rinsed with distilled water to remove impurities adhering to the raw material. Drying treatment at 50°C for 3 days removed excess moisture from the sample.

2.2. Experimental methods

2.2.1. Pretreatment

The raw material, tea twigs, was pretreated by drying in an oven at a temperature of 50-60°C until a moisture content of 10% was achieved. An electric grinder was used to crush the dried tea twigs into smaller particles. Sieving was performed manually to obtain a uniform quantity with a size between 170 and 200 mesh, which has been shown to be favorable for the physical synthesis of AC.

2.2.2. <u>Pyrolysis</u>

A high-temperature furnace equipped with heating elements, a thermocouple, and a nitrogen gas flow system was used for the pyrolysis process. Dried, crushed, and ground tea twigs (100 g) were placed in the center of the furnace and heated to a pyrolysis temperature of 400°C, followed by the flow of inert nitrogen gas at a rate of 5 mL min⁻¹ to maintain an inert atmosphere (Figure S1). Once the pyrolysis temperature was reached, the samples were held at the same temperature for 1 hour to determine the degree of combustion or mass loss due to pyrolysis. The yield of pyrolyzed tea twigs (tea twigs char) was calculated as the mass ratio of the pyrolyzed sample to the input raw material. The biochar produced from the carbonization process is then filtered to obtain biochar with a particle size of 170-200 mesh.

Before the samples are physically activated in the Arc Plasma, the biochar must be compacted using a sample press. To compact the samples, poly(acrylic acid) ($C_3H_4O_2$)_n, Sigma Aldrich, CAS Number 9003-01-4, is used as a binder, along with distilled water as a solvent and the filtered biochar. The ratio of biochar, binder, and distilled water is 1:0.1:0.5. The mixing of poly(acrylic acid) and distilled water are mixed and heated on a hotplate at 50°C until a slurry is formed. The biochar was then mixed with the slurry and thoroughly stirred. The mixture was dried in an oven at 80°C for 5 hours. The samples are then pressed using a sample press. The pressure applied during pressing is 40 bar, with a holding time of 2 min.

2.2.3. Activation

The pressed samples were subjected to physical activation using Arc Plasma (Figure 1). The samples were placed in a holder casing, and the sample holder motor was activated to bringeth the samples closer to the plasma torch. The parameters that influence physical activation are activation time and temperature. Each activated sample was treated for the same duration of 4 min. The choice of a 4-min activation time is based on the thermal plasma-influenced optimal pore formation during the etching process, which can take up to 5 min (Lim et al., 2023). Furthermore, the sample names for each variation were adjusted according to the temperature in the arc plasma during physical activation. The AC samples produced in this study include AC 600 (AC obtained from physical activation at 600°C), AC 700 (AC obtained from physical activation at 700°C), and AC 800 (AC obtained from physical activation at 800°C). Figure S2 shows a schematic of the activated carbon production process from tea twigs and physical activation with Arc Plasma.

2.3. Characterization

The physicochemical properties of the experimental samples were evaluated through a series of characterization studies. The samples were dried in an oven at 80°C for 4 hours before any testing procedures were carried out to remove the adsorbed moisture. The activated samples were characterized using SEM, BET, FTIR, and XRD. The morphology and topography of the samples were examined using SEM/EDS on a Hitachi SU-3500, Japan. Samples were prepared with gold coating at 18-25°C and observed at a magnification of X3000 under 10 kV. Specific surface area determination and porosity analysis were conducted using a Micromeritics TriStar II 3020 instrument. The nitrogen adsorption/desorption isotherms were measured at 77 K (-196°C) in the relative pressure range of 0.05<P/P₀<1.00 to characterize the textural parameters. The specific surface area (S_{BET}) and total pore volume (V_{TOT}) were calculated using the BET method at a relative pressure of 0.95. Before the experiments, the samples were vacuum-outgassed for 2 hours at 150°C to remove any adsorbed gases or moisture. All activated carbon samples were analyzed to identify the basic functional groups using Fourier transform infrared (FTIR) spectroscopy. Fourier transform infrared (FTIR) spectra were obtained using the standard attenuated total reflection (ATR) method in the range of 4000 to 500 cm⁻¹ (45 scans at a resolution of 2 cm⁻¹). The crystalline structure and degree of crystallinity of the activated carbons were examined using X-ray diffraction (XRD) with a SmartLab Rigaku, equipped with CuKa radiation (λ =1.5418 Å) and a step size of 0.050 from 5° to 110°. The supplied voltage was 40 kV with a current of 30 mA.

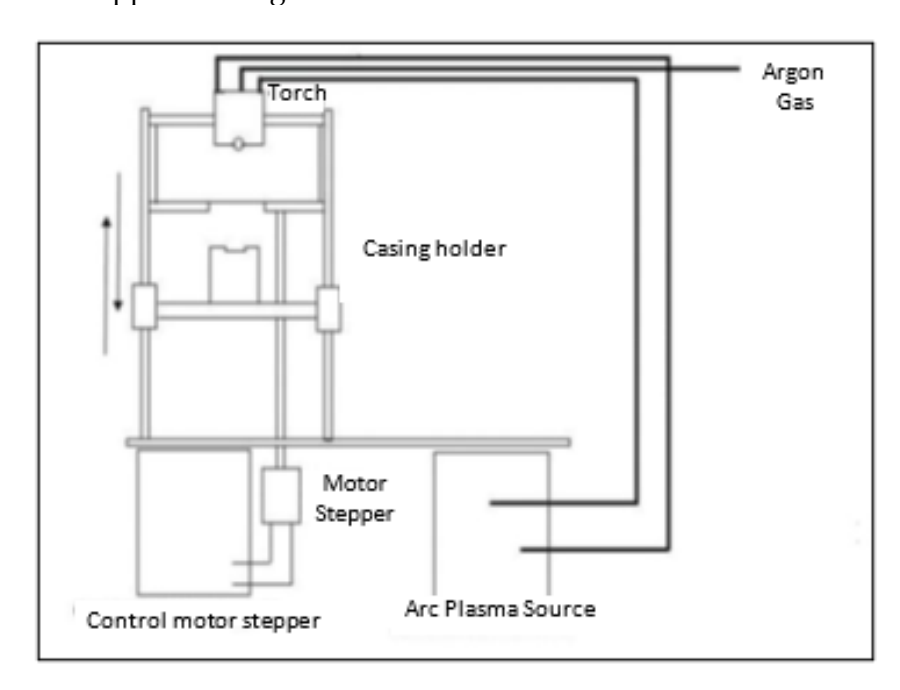


Figure 1 Schematic of Arc Plasma (scale 1:3)

The CO₂ adsorption test was conducted using Temperature-Programed Desorption of CO₂ (TPD-CO₂ Micromeritics Autochem III (USA), involving several stages: pretreatment, adsorption, and desorption. The purpose of pretreatment is to remove volatile substances or impurities that remain on the activated carbon surface. The temperature and duration of pretreatment were 150°C and 60 min, respectively. During the pretreatment process, helium gas was flowed at a rate of 50 cm³ min⁻¹. Klepel and Hunger (2005) investigated CO₂ adsorption through Temperature Programed Desorption of CO₂ using a helium gas flow rate of 50 cm³ min⁻¹ (Klepel and Hunger, 2005). This flow rate was adopted as the gas flow rate in this study. A 55 mg sample was loaded into the reactor and heated from room temperature to 150°C at a heating rate of 30°C min⁻¹ with a helium flow rate of 50 cm³ min⁻¹, and the sample was then treated at 150°C for 1 hour. The CO₂ gas flow was maintained at 50 cm³ min⁻¹ for sample pre-saturation at 40°C for 60 min. Subsequently, the sample was heated to 350°C at a heating rate of 10°C min⁻¹ until the desorption equilibrium was reached.

3. Results and Discussion

3.1. Yield of biochar and activated carbon

The heating temperature, process duration, and flow rate of inert gas influence carbonization. The carbonization process temperature plays a crucial role in the decomposition of organic compounds into pure carbon. Tabak et al. (2019) conducted thermal analysis (TGA) on tea twigs and identified three stages of decomposition: (1) at temperatures of 200-300°C, hemicellulose degradation occurs; (2) at 275-400°C, cellulose degradation takes place; and (3) at 250-500°C, lignin degradation occurs. The degradation of hemicellulose, cellulose, and lignin is necessary to achieve a high carbon content in biochar, as this increases pore formation (Panahi et al., 2020, Meyer et al., 2011). Therefore, a temperature of 400°C was chosen as the carbonization temperature in this study, which was maintained for 1 h. Meanwhile, a temperature of 500°C is less optimal for carbonization as it may result in biochar with lower carbon content and yield. A temperature of 300°C was also not selected for carbonization because the pore formation at this temperature was not yet optimal (Panwar et al., 2019).

Table S1 shows the yield of activated carbon. The carbonization process produces biochar with an approximate yield of 35%. The expected yield from carbonizing biomass samples made from wood, under identical temperature and operational conditions, ranges from 34% to 49% (Mukherjee et al., 2022; Titiladunayo et al., 2012). This indicates that the research findings fall within the range of anticipated yield. Nitrogen gas is flowed at a rate of 5 mL min⁻¹ during the carbonization process to provide an inert atmosphere that prevents oxidation of the biomass. This is crucial to ensure that the carbon produced does not oxidize back into more volatile compounds or ash. The nitrogen gas flow helps remove volatile gases from the reactor, thereby enhancing the final carbon product purity. During the physical activation process, mass loss occurs due to the evaporation of residual water, volatile compounds, and lignin degradation. Lignin is completely degraded at temperatures between 160°C and 900°C (Mahmoud and Ahmed, 2020; Tabak et al., 2019). Therefore, the mass loss during physical activation is also influenced by lignin degradation, which affects the yield values obtained.

Table S1 also presents the yield values from previous studies on the production of activated carbon. As indicated in Table S1, both the activation temperature and time are crucial factors in determining the yield of activated carbon. In the study by Ogungbenro et al. (2018), activated carbon was produced from date seeds through a carbonization process followed by physical activation using CO₂ gas as the oxidizing agent (Table S1). (Ogungbenro et al., 2018) The activation temperature in that study was varied between 600°C and 900°C, and the yield of activated carbon decreased as the temperature increased. Ogungbenro et al. (2018) attributed this reduction in yield to the further decomposition of the lignocellulosic chemical components of the date seeds (Ogungbenro et al., 2018). Their findings indicated that 800°C was the optimal activation temperature in a CO₂ atmosphere.

In the current study, physical activation was carried out using Arc plasma, with argon gas acting as the plasma source and protecting the material from oxidation during the activation process. The yields achieved from activation temperatures ranging from 600°C to 800°C were between 83-90%, significantly higher than those obtained with CO₂ gas activation, as reported by Ogungbenro et al. (2018) (Table S1). The use of Arc Plasma for physical activation resulted in higher yields compared with the use of an electric furnace. Additionally, the activation time played a critical role in determining the activated carbon yield.

In addition to the activation temperature, the activation time influences the yield capacity of the sample. The longer the sample is activated, the more the carbon content and volatile matter degrade and vaporize, while other minerals remain. Activation with Arc Plasma can be performed with a shorter activation time compared with that of an electric furnace. The results show that activation with Arc Plasma at 700°C for 4 min produces the highest yield (90%) compared with that in previous studies.

Arc plasma activation offers the advantage of higher yield values due to the shorter activation time and the ability to generate heat more quickly compared to electric furnace. The decrease in carbon content during activation affects not only the yield of activated carbon but also its adsorption capacity. Additionally, the polar nature of AC, which arises from the reactivity of surface functional groups formed by elemental deposits from the precursor, plays an important role in the AC adsorption performance. The presence of functional groups in tea twigs and the resulting activated carbon can be investigated using Fourier transform infrared (FTIR) techniques and will be discussed in the following section.

The other studies presented in Table S1 show high ACY values, ranging from 71 to 78%. The role of chemical activation agents is crucial in achieving high yield values, as reported in previous studies where the yield of activated carbon from chemical activation processes was around 35-78% (Table S1). The high yield values from chemical activation processes are likely due to the treatments applied during the production of activated carbon. Studies that support high activated carbon yields typically involve mixing the raw materials with activation agents before proceeding with carbonization at temperatures of 600-900°C for 1-2 hours. Treatment with activation agents during activated carbon production affects the yield values produced. However, few studies have reported activated carbon production through carbonization followed by physical activation using CO2 or steam followed by nitrogen gas flow. This study demonstrates activated carbon production through carbonization followed by physical activation using Arc Plasma with an inert Argon gas flow to generate plasma and protect the material from oxidation during the activation process. The yield values obtained in this study are higher than those obtained in previous studies that used a furnace with CO₂ gas flow for physical activation, and the yield values in this study are also higher than those obtained from activated carbon using chemical activation agents. This indicates that activated carbon production with Arc Plasma results in lower carbon and volatile matter loss, leading to higher yields.

3.2. Spectroscopic Analysis

The CO₂ adsorption capacity of AC can be observed through its functional groups. Fourier transform infrared (FTIR) transmission spectroscopy was conducted to obtain the wavenumber values indicating functional groups in the tea twigs and activated carbon samples. Tea twigs that have not undergone pyrolysis or activation exhibit more absorption bands than the samples with activated carbon. This is indicative of the lignocellulosic nature of the tea twigs and the presence of various functional groups, such as alkenes, esters, aromatics, alkanones, alcohols, hydroxyl groups, ethers, and carboxyl groups (Putri et al., 2025). The IR absorption band at 3654 cm⁻¹ signifies the presence of hydroxyl groups (OeH stretching between 3601 and 3317 cm⁻¹) in the tea twigs.

Functional groups that can enhance CO₂ adsorption include hydroxyl groups (O-H) with wavenumbers between 3200-3700 cm⁻¹, aromatic groups (C=C) with wavenumbers ranging from 1566-1650 cm⁻¹, and C-O groups with wavenumbers between 1050-1310 cm⁻¹. The FTIR results

indicate that all samples subjected to physical activation at AC 600, AC 700, and AC 800 contain hydroxyl (O-H) groups (Figure 2). The role of hydroxyl (O-H) groups in CO₂ adsorption is to form hydrogen bonds with CO₂ molecules. These hydrogen bonds enhance the interaction between the surface of the activated carbon and CO₂ molecules. AC 800 shows a higher number of wave numbers and greater wave number values for hydroxyl (O-H) groups than the samples activated at 600°C and 700°C.

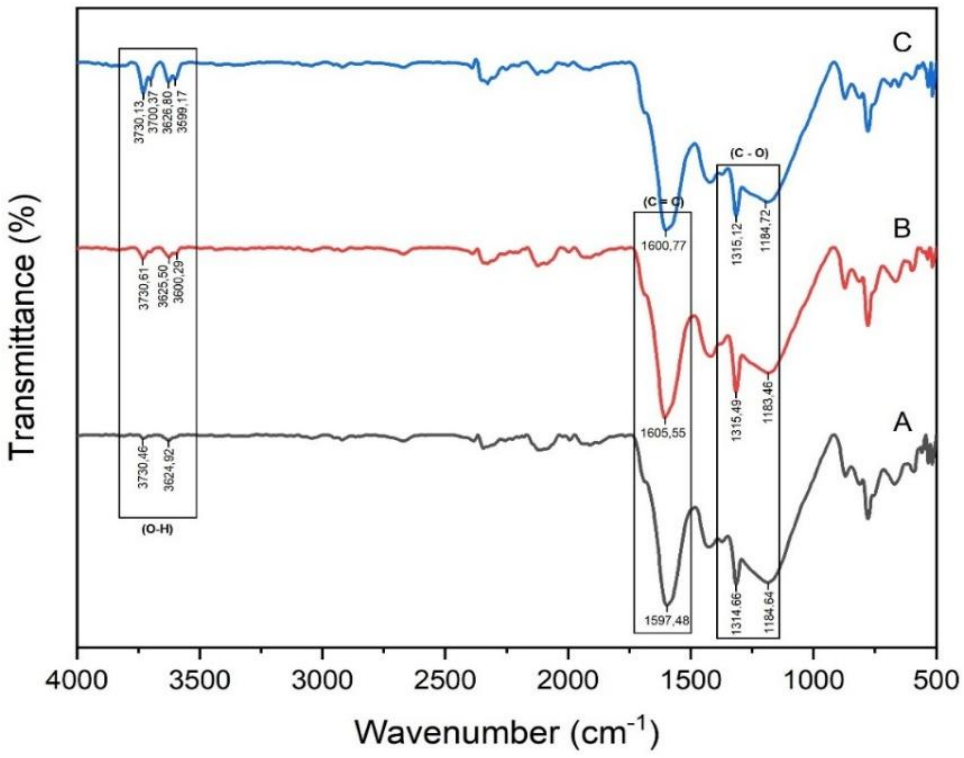


Figure 2 Functional groups of arc plasma-activated carbon at (A) 600°C, (B) 700°C, and (C) 800°C

In addition, each sample contains aromatic (C=C) functional groups that possess electrophilic properties that are beneficial for CO_2 adsorption. This is because CO_2 acts as a nucleophile and reacts with the electrophilic sites on the aromatic ring. Furthermore, each sample has C-O functional groups that can impart a negative charge to the carbon surface, enhancing electrostatic interactions and bonding with CO_2 molecules. The AC 800 shows a significant wave number for the C-O functional group. Each sample demonstrates the ability to adsorb CO_2 based on its functional group content.

3.3. Diffraction Analysis Pattern

Figure 3 shows the diffraction patterns from the X-ray diffraction (XRD) analysis for samples. For reference, the XRD pattern of activated carbon typically displays two diffraction peaks at 2-theta = 24-25° and 43° (Fahmi Puteri et al., 2021; Omri and Benzina, 2012). The samples treated with the Arc Plasma at 600°C, 700°C, and 800°C exhibit a diffraction peak at 2-theta = 24°, indicating that the samples align well with the activated carbon XRD diffraction pattern. Additionally, the XRD patterns for each sample showed relatively broad and less sharp peaks, indicating the presence of an amorphous carbon structure. A weak peak is observed at 2-theta = 43°, which is likely caused by diffraction from the amorphous structure, indicating that physical activation decreases the random structure (Borah et al., 2015).

Table S2 compares the FWHM values and crystal sizes at the peak of 2-theta = 24° . The carbon activated at relatively higher temperatures (around 800° C) yields smaller crystal size values than the carbon activated at 600° C and 700° C. The crystal size value of the obtained activated carbon sample is approximately 0.36 nm. This value is larger than that of graphite (0.335 nm). The increase

in temperature during physical activation indicates a widening of the peak and a decrease in crystal size, corresponding to an increase in porosity and a more amorphous structure (Chatterjee et al., 2020). The sample activated at 800°C has the largest FWHM and the smallest crystal size, indicating the highest porosity among the three samples. This phenomenon is consistent with the literature on carbon produced from corncob (Sun and Webley, 2010). The increase in the surface area of activated carbon leads to a decrease in the crystal size value, which is caused by the densification of the structure of the material (Jjagwe et al., 2021). These XRD results align with the BET characterization results, showing that the activated carbon sample at 800°C has a larger surface area than those activated at 600°C and 700°C.

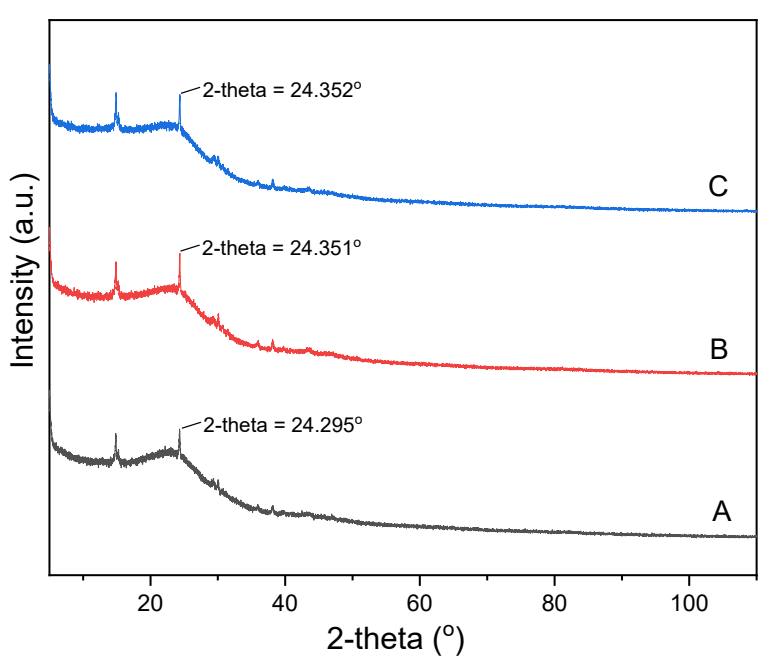


Figure 3 Diffraction patterns of arc plasma-activated carbon at (A) 600°C, (B) 700°C, and (C) 800°C

3.4. Morphology Analysis

SEM characterization was used to obtain morphological and topographical images of the tea twigs and produced activated carbons. Figure S3 (a) shows the surface of the raw material, which remains non-porous due to the absence of thermal treatment. Biomass raw materials contain cellulose and lignin, which influence the pore surface characteristics and activated carbon surface area. During the carbonization process, thermal decomposition occurs, in which lignin and cellulose undergo a series of reactions that transform these organic substances into carbon, resulting in biochar. Elemental pores in the biochar sample are generated through the removal of most non-carbon elements during carbonization, yielding a monolithic carbon framework. The thermal decomposition of biomass during carbonization also generates tar, which clogs pores. As shown in Figure S3(b), the thermal breakdown of biomass produces tar that continues to obstruct the formed pores. Extensive tar formation during carbonization leads to biochar with a low specific surface area from tea twigs. As the biomass decomposes and volatile compounds are released during carbonization, the material's carbon content increases, whereas its oxygen and hydrogen contents decrease. This resulted in carbon-rich biochar, making it a promising material for use as an adsorbent.

Figure S4 shows the well-formed and distinct pores in the activated carbon. As the activation temperature increased from 600°C to 700°C and then to 800°C, the development of porosity became more evident (Figure S4 (a-c)). The figure demonstrates the gradual formation of pores as the activation temperature increases. Pore formation is partial at lower temperatures, but broader micropores begin to develop as the temperature increases. Moreover, pore creation in AC can also

be attributed to etching caused by the free electrons generated during the process. Higher electric current settings during arc plasma activation lead to the production of more electrons and greater heat generation. Selective etching occurs as the heat increases, which optimizes the removal of volatile impurities and eliminates hydrocarbon contaminants from the biochar, thus expanding the cavity structure. Arc plasma activation enhances the pore structure of the AC, and larger, well-formed pores are visible on the surface of the AC 800 sample (Figure S4 (c)). Higher activation temperatures cause pore collapse. These well-developed pores are essential for improving the CO₂ adsorption capacity of activated carbon.

3.5. Analysis of porosity and surface area

The characteristics of the pore surface in activated carbon can be determined through analysis using the Brunauer-Emmett-Teller (BET) method. The BET results for the AC samples indicate that the largest pore surface area was obtained from AC 800 (Table 1).

Table 1 Results of the BET characterization

No	Samples	$S_{BET} (m^2 g^{-1})$	V_{total} (cm ³ g ⁻¹)	V_{micro} (cm ³ g ⁻¹)	V_{meso} (cm ³ g ⁻¹)	D (nm)
1	Biochar	13.920	0.041	0.040	0.001	12.340
2	AC 600	80.189	0.115	0.096	0.019	2.737
3	AC 700	84.876	0.138	0.072	0.066	2.340
4	AC 800	86.668	0.157	0.039	0.118	2.118

 S_{BET} = Specific surface area calculated using the BET method

 V_{tota} = Total pore volume calculated at P/P₀ = 0.99

D = Pore size (nm)

 V_{micro} = Micropore volume calculated using the t-plot method

 V_{meso} = mesopore volume calculated from V_{total} V_{micro}

Table 1 illustrates the increase in surface area and pore volume of biochar produced through carbonization and biochar activated with Arc Plasma at 600°C, 700°C, and 800°C. The carbonized biochar has a surface area of 13.920 m² g⁻¹. The properties of the adsorbent raw materials, including the volatile matter content in biomass precursors, have a significant impact on porosity development, although they do not influence the adsorption properties due to the creation of inert sites within the activated carbon pores (Putri et al., 2025). The presence of volatile matter in the raw material can be eliminated during the carbonization process, as the tea twigs undergo thermal decomposition, leading to the formation of tar that blocks the pores and reduces the surface area (Karume et al., 2023). In a study by Putri et al. (2025), the raw material of tea twigs had a high volatile matter content of 76.59% (Putri et al., 2025). However, volatile matter can be eliminated during the carbonization process, as the tea twigs undergo thermal decomposition during carbonization. Biochar from tea twigs has a low surface area due to the relatively high formation of tar during carbonization, which is a result of thermal decomposition to remove the tea twigs' relatively high volatile matter content. Thus, the formation of relatively high tar during carbonization results in the blocking of pores, leading to a low biochar surface area (Karamah et al., 2019).

Tea twigs have a low non-volatile content and a flammable physical structure, both of which contribute to a low ash content of 1.69% (Putri et al., 2025). A precursor with a low ash content typically produces activated carbon with improved porosity because fewer inert materials hinder pore formation during the activation process. The reduced ash content allows a greater amount of carbon to contribute to pore formation, leading to an effective pore size suitable for adsorption (Malhotra et al., 2018). The results of the study indicate that activated carbon samples from AP activation exhibit pore sizes ranging from 2.1 to 2.7 nm, which are similar to those of micropores. The relatively low specific surface area, despite the pore size being close to that of micropores, is likely due to incomplete pore formation during AP activation. Activation time plays a critical role in pore development, as noted by Ogungbenro et al. (2018). As the activation time increases, more

carbon and volatile matter are degraded and vaporized. Short activation times with Arc Plasma lead to incomplete pore formation, making the activation process less effective, even though the resulting samples have pore sizes similar to those of micropores. However, shorter activation times result in higher yields. Therefore, in this study, an activation time of 4 min was chosen to achieve optimal micropore development, as the etching process influenced by thermal plasma takes up to 5 min (Lim et al., 2023).

The physical or thermal activation treatment using Arc Plasma results in increased surface area and pore volume, as well as changes in pore size on the activated carbon surface. This indicates that activation with arc plasma causes a greater increase in the porosity within the surface structure of the sample. As the activation process begins, pore development gradually occurs. At low combustion temperatures, pore development occurs partially, and as the combustion temperature increases, micropore development becomes wider, as indicated by the larger surface area and pore volume (see Table 1).

Utilizing Arc Plasma for physical or thermal activation in the production of activated carbon is an innovation, as improvements in surface area have traditionally been achieved through chemical activation using basic or acidic activating agents such as KOH, NaOH, ZnCl₂, or H₃PO₄. There is currently no literature that describes the mechanism of pore formation using arc plasma; however, arc plasma is a type of thermal plasma generated through gas ionization. Argon gas is used as an inert gas in the activation of biochar with argon plasma. When ionization occurs between Ar (Ar) inert gas under the actantial difference between the anode and cathode with a pulsed current, electrons are released from Ar atoms, generating positive Argon ions (Ar⁺) and free electrons (e⁻). Carbon is a conductive material with electrons moving within its structure. When the carbon material is exposed to electrons, the free electrons in the carbon respond by moving, creating eddy currents. These currents flow in a closed circular pattern within the conductor, causing resistance and heat release. When the size of the biochar is larger than the depth of the skin effect of the generated current, the biochar surface can be heated locally. This thermal effect leads to pore formation on the biochar surface, resulting in a porous activated carbon material. Additionally, etching caused by the generated free electrons can cause pore formation in activated carbon. The higher the electric current setting, the more electrons generated and the greater the heat produced. This study applied temperatures of 600°C, 700°C, and 800°C for physical activation. The increase in the activation temperature positively affects the increase in the surface area. Activated carbon treated with Arc Plasma at temperature of 800°C achieved a surface area of 86.668 m² g⁻¹, a pore volume of 0.157 cm³ g⁻¹, and a pore size of 2.118 nm. This surface area value is larger than those of the other samples. The increase in activation temperature can optimize the removal of volatile impurities and eliminate hydrocarbon contaminants from the biochar produced during carbonization, as well as enlarge the cavity structure, thereby increasing the surface area (Ramadhani, 2020; Yuliusman, 2015).

The pores in the biochar produced from carbonization are classified as mesopores based on pore size and volume, with a pore size of 12.340 nm and a pore volume of 0.041 cm³ g⁻¹. In contrast, activated carbon samples subjected to physical activation are classified as micropores, with pore sizes ranging from 2.118 to 2.727 nm and pore volumes ranging from 0.115 to 0.157 cm³ g⁻¹ (Phothong et al., 2021). Physically activated carbon samples exhibit a greater CO₂ adsorption capacity than biochar samples due to their smaller pore sizes. Pore sizes of 1-2.5 nm are optimal for gas adsorption, particularly for CO₂ (Chen et al., 2017). This will be discussed in the following section.

3.6. CO₂ Adsorption

The CO₂ adsorption capacity was determined using a Temperature Programed Desorption of CO₂ (TPD-CO₂). The adsorption capacity data for each sample, including those obtained from carbonization and the activated carbon samples treated with Arc Plasma at activation temperature of 600°C, 700°C, and 800°C, can be seen in Table 2.

		I		, , -	(- 0 /
	No	Samples	Specific surface	Pore volume	Pore size	CO ₂ adsorption
_			area (m² g-1)	$(cm^3 g^{-1})$	(nm)	(mmol/g)
	1	Biochar	13.920	0.041	12.340	0.354
	2	AC 600	80.189	0.115	2.737	1.816
	3	AC 700	84.876	0.138	2.340	1.959
	4	AC 800	86.668	0.157	2.118	2.057

Table 2 Adsorption of CO₂ from biochar, AC 600, AC 700, and AC 800 (in mmol g⁻¹)

The mechanism of the adsorption process can be explained in two ways: physical and chemical adsorption. Physical adsorption occurs because of factors such as surface area, pore volume, and pore size. Table 2 presents the physical characteristics of activated carbon that influence CO₂ adsorption capacity. The larger the surface area of activated carbon, the more active sites are available for the adsorption of CO₂ molecules. Table 2 shows a significant increase in the surface area from biochar (13.920 m² g⁻¹) to physically activated carbon using Arc Plasma at temperature of 800°C (86.668 m² g⁻¹). The growth in surface area is directly related to the improvement in CO₂ adsorption capacity, with biochar showing a capacity of 0.354 mmol g⁻¹, while the activated carbon sample treated with Arc Plasma at 800°C reaches 2.057 mmol g⁻¹. This study demonstrates that activated carbon with a larger surface area can improve its ability to adsorb CO₂.

Figure S5 shows the relationship between the surface area (m^2 g⁻¹) and CO₂ adsorption capacity (mmol g⁻¹), indicating that a greater surface area leads to increased CO₂ adsorption. Additionally, a larger pore volume allows more CO₂ molecules to be adsorbed into the activated carbon structure. The data in Table 4 reveal an increase in pore volume from 0.041 cm³ g⁻¹ in the biochar to 0.157 cm³g⁻¹ in the AC 800 sample. Increasing the pore volume contributes to the enhanced CO₂ adsorption capacity. A larger pore volume provides sufficient space for CO₂ molecules to enter and become trapped.

Figures S5 and S6 demonstrate that as the activation temperature increases, the CO₂ adsorption capacity also increases in a nearly linear manner. The increase in temperature accelerates the collision frequency of molecules, resulting in more effective reactions, or strengthens the van der Waals forces, enabling CO₂ to diffuse more effectively into the reaction sites. The results of this study also reveal a nearly linear correlation between CO₂ adsorption capacity and specific surface area and pore volume, as shown in Figures S3 and S4. These findings align with previous reports that highlight the crucial role of specific surface area and pore volume in CO₂ absorption (Nurfarhana et al., 2023; Yuliusman et al., 2019). As the adsorbent's specific surface area increases, a greater amount of adsorbate can be bound to the adsorbent's pores (Sudibandriyo and Putri, 2024; Yuliusman et al., 2019).

Figure S6 shows the effect of pore volume on CO₂ adsorption capacity indicating that as pore volume increases, more CO₂ can be adsorbed. Activated carbon with mesopore sizes (around or larger than 30 Å or equivalent to 3 nm) is more suitable for liquid-phase applications, whereas smaller pore sizes (10 to 25 Å or equivalent to 1–2.5 nm) are appropriate for gas-phase applications. However, the AC 600 sample with a pore size of 2.737 nm is still considered suitable for gas adsorption. Smaller pore sizes, which are closer to the size of CO₂ molecules, enhance the interaction between CO₂ molecules and pore walls, thereby increasing adsorption capacity.

Table 3 summarizes the CO₂ adsorption capacity of the activated carbon samples, comparing the data with those in the existing literature. The activated carbon sample with the highest CO₂ adsorption capacity in this study is 2.057 mmol g⁻¹, which is consistent with the CO₂ adsorption capacity of commercial activated carbon (Table 3). Moreover, Table 3 includes literature results showing that although activated carbon with smaller surface areas was used, its CO₂ adsorption capacity is still comparable to that of commercial activated carbon. In addition to the specific surface area, the pore size of the material influences the CO₂ adsorption capacity. Smaller pores generally exhibit higher CO₂ adsorption, and as the pore size increases, the CO₂ adsorption capacity tends to decrease (as seen in Table 2). These results are consistent with those of previous studies

(Chen et al., 2017). The pore size of the activated carbon samples derived from AP activation falls between 2.1 and 2.7 nm, which is near the micropore size range. Most CO₂ adsorption in activated carbon occurs within micropores (diameter: 2 nm). Smaller pores enable more CO₂ molecules to be adsorbed, as CO₂ molecules are more effectively trapped within the activated carbon, thus reducing the chances of gas escaping before complete absorption. Smaller pores can also reduce the CO₂ diffusion rate, thereby enhancing the adsorption efficiency and maximizing the adsorption capacity.

Figure 6 shows the interaction between CO_2 gas molecules and the adsorbent surface, as well as the energy required to release CO_2 from the surface. The curve presents peaks that indicate the temperature at which CO_2 desorbs from the surface. A higher peak indicates a stronger bond between CO_2 and the adsorbent surface, necessitating a higher desorption temperature. In contrast, a lower peak represents a weaker bond, enabling CO_2 to be released at a lower temperature. The peak at a lower temperature signifies physisorption, where CO_2 is held by weaker Van der Waals forces on the adsorbent surface. The peak at a higher temperature point to chemisorption, where CO_2 is more strongly attached through chemical bonds, requiring a higher temperature for desorption. The peak at a higher temperature points to chemisorption.

Table 3 Comparison of the Research Results

No	Authors	Raw materials	Specific surface area (m² g-¹)	CO ₂ adsorption capacity (mmol/g)	Adsorption conditions (P and T)
1	(Rashidi et al.(Rashidi	Commercially	717.22	1.84	1 bar, 50°C
	et al., 2014))	available			
		activated carbon			
2	(Eny Kusrini, 2017)	Graphite waste	8.49	2.737	3 bar, 45°C
			18.48	1.62	
			35.52	0.61	
3	(Joseph et al., 2017)	Oil palm fruit bunch	14.32	1.93	1 bar, 25°C
4	(Yıldız et al., 2019)	Chicken manure waste	22.22	1.95	1 bar, 25°C
5	(Ding and Liu, 2020)	Enteromorpha	60.2	0.52	1 bar, 25°C
6	(Ding and Liu, 2020)	Sargassum	291.8	1.05	1 bar, 25°C
4	AC 600 (in this study)	Tea twigs	80.189	1.816	1 bar, 40°C
	AC 700 (in this study)		84.876	1.959	
	AC 800 (in this study)		86.668	2.057	

The curves of samples AC 600, AC 700, and AC 800 show two distinct peaks, indicating the existence of homogeneous active sites. The curve with a higher sharp peak indicates that a significant amount of energy is required for CO₂ desorption, whereas the curve with a lower sharp peak requires less energy for desorption. These sharp peaks are evident across all samples, with the first peak corresponding to CO₂ release at a lower temperature (<200°C), indicating a minimal energy requirement consistent with physisorption. In contrast, the broader second peak signifies the presence of heterogeneous active sites. This second peak reflects a chemisorption phenomenon, where CO₂ is strongly bonded and desorbed at a higher temperature (>200°C). All samples exhibited a more pronounced chemisorption behavior during CO₂ adsorption, which was likely influenced by the adsorption temperature used.

CO₂ lacks a dipole moment but has a significant quadrupole moment. Its linear shape and polar bonds at both ends enable it to easily interact with active sites on the char surface (Goel et al., 2021). At lower adsorption temperatures, CO₂ molecules have reduced kinetic energy, making them more likely to be adsorbed and held on the adsorbent's surface. As a result, low temperatures are

generally used to improve CO₂ adsorption capacity, as shown in Table 6. While many studies have examined adsorption at room temperature, few have provided data on CO₂ adsorption capacities at temperatures higher than room temperature. The findings of this study indicate that a relatively high CO₂ adsorption capacity can be achieved at an adsorption temperature of 40°C. However, chemisorption mechanisms are the primary governing factor for adsorption at temperatures slightly above room temperature, as shown in Figure 6.

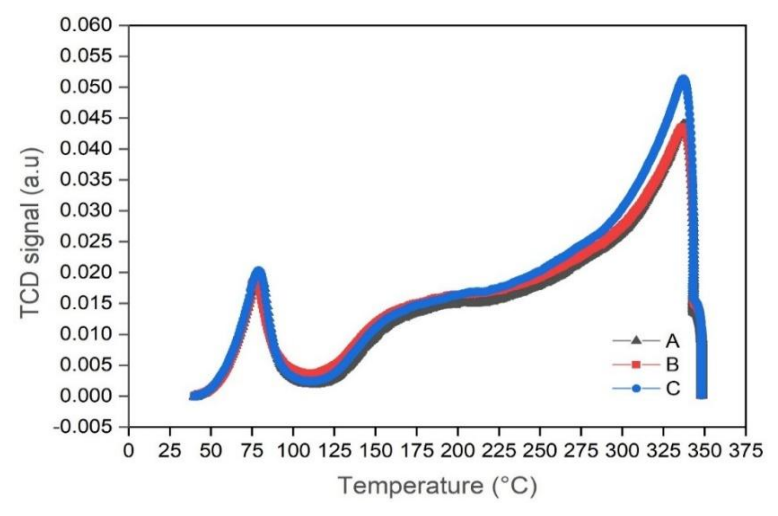


Figure 6 Temperature Programed Desorption of CO₂ (TPD-CO₂) curve of arc plasma-activated carbon at (A) 600°C, (B) 700°C, and (C) 800°C

At 40°C, adsorption starts due to the attractive forces between CO₂ molecules and the activated carbon surface. However, the van der Waals forces at play are relatively weak, which is reflected in the low and sharpness of the first peak. As the temperature increases during adsorption, the interaction between CO₂ molecules and the atoms or ions on the activated carbon surface strengthens, forming chemical bonds and heterogeneous active sites. A high desorption temperature is required to break these chemical bonds, as indicated by the higher and broader second peak. The chemisorption effect is more pronounced in all samples because the area under the second peak is larger than that under the first peak. All samples exhibited weak van der Waals interactions, but as the temperature rises during adsorption, stronger chemical bonds are formed between CO₂ molecules and the activated carbon surface. The results indicate that the adsorption temperature plays a crucial role in determining the adsorption mechanism.

The findings of this study are in agreement with earlier research on CO₂ adsorption performance, which demonstrated that CO₂ adsorption at lower temperatures enhances the physical adsorption efficiency. Physisorption is more effective at lower adsorption temperatures because it facilitates better trapping of CO₂ molecules within the smaller pores of activated carbon. Additionally, lower temperatures help preserve the stability and adsorption capacity of AC, which is essential for effective CO₂ adsorption (Zubbri et al., 2021; Huang et al., 2019).

4. Conclusions

This study investigates the production of activated carbon from tea branch biomass through a carbonization process followed by physical activation using arc plasma. The resulting activated carbon was analyzed to assess its pore characteristics, and CO₂ adsorption tests were conducted. The properties examined include surface area, morphological structure, presence of functional groups, and crystallinity of the activated carbon pores were examined. This research on activated carbon with Arc Plasma activation is a novel approach, and the findings demonstrate that the CO₂ adsorption capacity of the activated carbon derived from tea branch biomass through Arc Plasma activation is 2.057 mmol g⁻¹. Arc plasma presents advantages by reducing the activation time and

yielding activated carbon with a high adsorption capacity. In conclusion, the activated carbon adsorbent from tea branches, activated with Arc Plasma, shows great actantial for CO₂ adsorption applications, offering a short activation time. Further investigations are needed to explore the selectivity of CO₂ separation from gas streams and the performance of the material under various adsorption conditions, which will be the focus of future research.

Acknowledgments

The authors acknowledge the facilities and scientific and technical sunport from the Advanced Characterization Laboratories Serpong, National Research and Innovation Institute through E-Layanan Sains, Badan Riset dan Inovasi Nasional. The authors disclosed receipt of the following financial sunport for the research, authorship, and/or publication of this article: This research was funded and supported by Operational Assistance Program for State Universities – Doctoral Dissertation Research Program (Fiscal Year 2024), grant numbers NKB-975/UN2.RST/HKP.05.00/2024 and 350/PKS/WR III/UI/2024, which was granted by the Ministry of Education, Culture, Research, and Technology of the Republic of Indonesia.

Author Contributions

Ary Mauliva Hada Putri and Yuswan Muharam was responsible for the conceptualization of the study, development of the methodology, conducting the experimental investigation, data curation, formal analysis, and writing the original draft of the manuscript. Rakhael Cahya Nugraheni Budiharja contributed to the visualization of the data and assisted in reviewing and editing the manuscript. Benni F. Ramadhoni participated in the experimental methodology, provided necessary resources, and supported validation of the results. Yuliusman supervised the research and contributed to the critical revision and editing of the manuscript. Yuswan Muharam led the project administration, provided supervision throughout the study, and secured research funding.

Conflict of Interest

The authors have no conflicts of interest to declare

References

Amer, M & Elwardany, A 2020, 'Biomass carbonization', in Mansour Al, Q, Ahmad, EK & Hakan Serhad, S (eds), *Renewable energy*, IntechOpen, Rijeka, London, England, https://doi.org/10.5772/intechopen.90480 Badan Pusat Statistik (BPS) 2023, *Indonesia tea statistics*, Badan Pusat Statistik, Jakarta, Indonesia

Boonpoke, A, Chiarakorn, S, Laosiripojana, N, Towprayoon, S & Chidthaisong, A 2010, 'Synthesis of activated carbon and MCM-41 from bagasse and rice husk and their carbon dioxide adsorption capacity', *Journal of Sustainable Energy & Environment*, vol. 2, pp. 77-81, https://api.semanticscholar.org/CorpusID:53580943

Borah, L, Goswami, M & Phukan, P 2015, 'Adsorption of methylene blue and eosin yellow using porous carbon prepared from tea waste: Adsorption equilibrium, kinetics and thermodynamics study', *Journal of Environmental Chemical Engineering*, vol. 3, pp. 1018–1028, https://doi.org/10.1016/j.jece.2015.02.013

Chatterjee, R, Sajjadi, B, Chen, WY, Mattern, DL, Hammer, N, Raman, V & Dorris, A 2020, 'Effect of pyrolysis temperature on physicochemical properties and acoustic-based amination of biochar for efficient CO₂ adsorption', *Frontiers in Energy Research*, vol. 8, https://doi.org/10.3389/fenrg.2020.00085

Chen, L, Watanabe, T, Kanoh, H, Hata, K & Ohba, T 2017, 'Cooperative CO₂ adsorption promotes high CO₂ adsorption density over wide optimal nanopore range', *Adsorption Science & Technology*, vol. 36, pp. 625–639, https://doi.org/10.1177/0263617417713573

Ding, S & Liu, Y 2020, 'Adsorption of CO₂ from flue gas by novel seaweed-based KOH-activated porous biochars', *Fuel*, vol. 260, article 116382, https://doi.org/10.1016/j.fuel.2019.116382

Eliasson, J & Carlsson, V 2020, Agricultural waste and wood waste for pyrolysis and biochar: An assessment for Rwanda, Independent thesis basic level (degree of bachelor), Student thesis

Fahmi Puteri, P, Cucun Alep, R & Yohanes, M 2021, 'Karakterisasi karbon aktif kulit singkong (Manihot esculenta Crantz) berdasarkan variasi konsentrasi H3PO4 dan lama waktu aktivasi' (Characterization of cassava peel (Manihot esculenta Crantz) activated carbon based on variations in H3PO4 concentration and activation time), *Indonesian Journal of Chemical Analysis*, vol. 4, no. 2, pp. 72–81, https://doi.org/10.20885/ijca.vol4.iss2.art4

Goel, C, Mohan, S & Dinesha, P 2021, 'CO₂ capture by adsorption on biomass-derived activated char: A review', *Science of The Total Environment*, vol. 798, article 149296, https://doi.org/10.1016/j.scitotenv.2021.149296

Gomez-Delgado, E, Nunell, G, Cukierman, AL & Bonelli, P 2022, 'Agroindustrial waste conversion into ultramicroporous activated carbons for greenhouse gases adsorption-based processes', *Bioresource Technology Reports*, vol. 18, article 101008, https://doi.org/10.1016/j.biteb.2022.101008

González-García, P, Centeno, TA, Urones-Garrote, E, Ávila-Brande, D & Otero-Díaz, LC 2013, 'Microstructure and surface properties of lignocellulosic-based activated carbons', *Applied Surface Science*, vol. 265, pp. 731–737, https://doi.org/10.1016/j.apsusc.2012.11.092

Gundogdu, A, Duran, C, Senturk, HB, Soylak, M, Imamoglu, M & Onal, Y 2013, 'Physicochemical characteristics of a novel activated carbon produced from tea industry waste', *Journal of Analytical and Applied Pyrolysis*, vol. 104, pp. 249–259, https://doi.org/10.1016/j.jaap.2013.07.008

Gundogdu, A, Duran, C, Senturk, HB, Soylak, M, Ozdes, D, Serencam, H & Imamoglu, M 2012, 'Adsorption of phenol from aqueous solution on a low-cost activated carbon produced from tea industry waste: Equilibrium, kinetic, and thermodynamic study', *Journal of Chemical & Engineering Data*, vol. 57, pp. 2733–2743, https://doi.org/10.1021/je300597u

Guo, Y, Sun, J, Wang, R, Li, W, Zhao, C, Li, C & Zhang, J 2021, 'Recent advances in potassium-based adsorbents for CO2 capture and separation: A review', *Carbon Capture Science & Technology*, vol. 1, article 100011, https://doi.org/10.1016/j.ccst.2021.100011

Han, J, Zhang, L, Zhao, B, Qin, L, Wang, Y & Xing, F 2019, 'The N-doped activated carbon derived from sugarcane bagasse for CO₂ adsorption', *Industrial Crops and Products*, vol. 128, pp. 290–297, https://doi.org/10.1016/j.indcrop.2018.11.028

Heidarinejad, Z, Dehghani, MH, Heidari, M, Javedan, G, Ali, I & Sillanpää, M 2020, 'Methods for preparation and activation of activated carbon: A review', *Environmental Chemistry Letters*, vol. 18, pp. 393–415, https://doi.org/10.1007/s10311-019-00955-0

Huang, G-G, Liu, Y-F, Wu, X-X & Cai, J-J 2019, 'Activated carbons prepared by the KOH activation of a hydrochar from garlic peel and their CO₂ adsorption performance', *New Carbon Materials*, vol. 34, pp. 247–257, https://doi.org/10.1016/S1872-5805(19)60014-4

International Energy Agency (IEA) 2023, CO₂ emissions in 2023, International Energy Agency (IEA), Paris Iqbaldin, MNM, Khudzir, I, Azlan, MIM, Zaidi, AG, Surani, B & Zubri, Z 2013, 'Properties of coconut shell activated carbon', *Journal of Tropical Forest Science*, vol. 25, pp. 497-503, https://jtfs.frim.gov.my/jtfs/article/view/460

Jjagwe, J, Olupot, PW, Menya, E & Kalibbala, HM 2021, 'Synthesis and application of granular activated carbon from biomass waste materials for water treatment: A review', *Journal of Bioresources and Bioproducts*, vol. 6, no. 4, pp. 292–322, https://doi.org/10.1016/j.jobab.2021.03.003

Joseph, CG, Quek, KS, Daud, WMAW & Moh, PY 2017, 'Physical activation of oil palm empty fruit bunch via CO₂ activation gas for CO₂ adsorption', *IOP Conference Series: Materials Science and Engineering*, vol. 206, article 012003, https://doi.org/10.1088/1757-899X/206/1/012003

Karamah, EF, Anindita, L, Amelia, D, Kusrini, E & Bismo, S 2019, 'Tofu industrial wastewater treatment with ozonation and the adsorption method using natural zeolite', *International Journal of Technology*, vol. 10, no. 8, pp. 1498–1504, https://doi.org/10.14716/ijtech.v10i8.3471

Karume, I, Bbumba, S, Tewolde, S, Mukasa, IHZT & Ntale, M 2023, 'Impact of carbonization conditions and adsorbate nature on the performance of activated carbon in water treatment', *BMC Chemistry*, vol. 17, article 162, https://doi.org/10.1186/s13065-023-01091-1

Klepel, O & Hunger, B 2005, 'Temperature-programmed desorption (TPD) of carbon dioxide on alkalimetal cation-exchanged faujasite type zeolites', *Journal of Thermal Analysis and Calorimetry*, vol. 80, pp. 201-206, https://doi.org/10.1007/s10973-005-0636-3

Kuptajit, P, Sano, N, Nakagawa, K & Suzuki, T 2021, 'A study on pore formation of high surface area activated carbon prepared by microwave-induced plasma with KOH (Miwp-KOH) activation: Effect of temperature-elevation rate', *Chemical Engineering and Processing - Process Intensification*, vol. 167, article 108511, https://doi.org/10.1016/j.cep.2021.108511

Kusrini, E, Sasongko, AK, Nasruddin & Usman, A 2017, 'Improvement of carbon dioxide capture using graphite waste/Fe3O4 composites', *International Journal of Technology*, vol. 8, no. 8, pp. 1436-1444, https://doi.org/10.14716/ijtech.v8i8.697

Lai, JY & Ngu, LH 2024, 'Post-combustion carbon dioxide adsorption of concurrent activated and surface modified palm kernel shell-derived activated carbon', *Greenhouse Gases: Science and Technology*, vol. 14, pp. 492-525, https://doi.org/10.1002/ghg.2274

Lai, JY, Ngu, LH & Hashim, SS 2021, 'A review of CO_2 adsorbents performance for different carbon capture technology processes conditions', *Greenhouse Gases: Science and Technology*, vol. 11, pp. 1076-1117, https://doi.org/10.1002/ghg.2112

Lim, C, Kwak, CH, Jeong, SG, Kim, D & Lee, YS 2023, 'Enhanced CO₂ adsorption of activated carbon with simultaneous surface etching and functionalization by nitrogen plasma treatment', *Carbon Letters*, vol. 33, pp. 139-145, https://doi.org/10.1007/s42823-022-00410-1

Luo, Y, Wang, K & Fei, L 2020, 'The effects of activation conditions on physical properties of activated carbon', *Bioresources*, vol. 15, pp. 7640-7647, https://doi.org/10.15376/biores.15.4.7640-7647

Malhotra, M, Suresh, S & Garg, A 2018, 'Tea waste derived activated carbon for the adsorption of sodium diclofenac from wastewater: Adsorbent characteristics, adsorption isotherms, kinetics, and thermodynamics', *Environmental Science and Pollution Research*, vol. 25, pp. 32210-32220, https://doi.org/10.1007/s11356-018-3148-y

Meyer, S, Glaser, B & Quicker, P 2011, 'Technical, economical, and climate-related aspects of biochar production technologies: A literature review', *Environmental Science & Technology*, vol. 45, no. 22, pp. 9473-9483, https://doi.org/10.1021/es201792c

Mukherjee, A, Patra, BR, Podder, J & Dalai, AK 2022, 'Synthesis of biochar from lignocellulosic biomass for diverse industrial applications and energy harvesting: Effects of pyrolysis conditions on the physicochemical properties of biochar', *Frontiers in Materials*, vol. 9, https://doi.org/10.3389/fmats.2022.870184

Nurfarhana, MM, Asikin-Mijan, N & Yusoff, SFM 2023, 'Porous carbon from natural rubber for CO_2 adsorption', *Materials Chemistry and Physics*, vol. 308, article 128196, https://doi.org/10.1016/j.matchemphys.2023.128196

Ogungbenro, AE, Quang, DV, Al-Ali, KA, Vega, LF & Abu-Zahra, MRM 2018, 'Physical synthesis and characterization of activated carbon from date seeds for CO₂ capture', *Journal of Environmental Chemical Engineering*, vol. 6, pp. 4245-4252, https://doi.org/10.1016/j.jece.2018.06.030

Omri, A & Benzina, M 2012, 'Characterization of activated carbon prepared from a new raw lignocellulosic material: Ziziphus spina-christi seeds', *Journal de la Société Chimique de Tunisie*, vol. 14, pp. 175-183, http://www.sctunisie.org/pdf/JSCT-v14-22.pdf

Panahi, HKS, Dehhaghi, M, Ok, YS, Nizami, AS, Khoshnevisan, B, Mussatto, SI, Aghbashlo, M, Tabatabaei, M & Lam, SS 2020, 'A comprehensive review of engineered biochar: Production, characteristics, and environmental applications', *Journal of Cleaner Production*, vol. 270, article 122462, https://doi.org/10.1016/j.jclepro.2020.122462

Panwar, NL, Pawar, A & Salvi, BL 2019, 'Comprehensive review on production and utilization of biochar', *SN Applied Sciences*, vol. 1, article 168, https://doi.org/10.1007/s42452-019-0172-6

Phothong, K, Tangsathitkulchai, C & Lawtae, P 2021, 'The analysis of pore development and formation of surface functional groups in bamboo-based activated carbon during CO2 activation', *Molecules*, vol. 26, article 5641, https://doi.org/10.3390/molecules26185641

Plaza-Recobert, M, Trautwein, G, Pérez-Cadenas, M & Alcañiz-Monge, J 2017, 'Preparation of binderless activated carbon monoliths from cocoa bean husk', *Microporous and Mesoporous Materials*, vol. 243, pp. 28-38, https://doi.org/10.1016/j.micromeso.2017.02.015

Putri, AMH, Ramadhoni, BF, Radias, MSH, Riyadi, FA, Alam, MZ & Muharam, Y 2025, 'Performance of activated carbon derived from tea twigs for carbon dioxide adsorption', *Current Research in Green and Sustainable Chemistry*, vol. 10, article 100440, https://doi.org/10.1016/j.crgsc.2024.100440

Ramadhani, LF, Nurjannah, IM, Yulistiani, R & Saputro, EA 2020, 'Review: Teknologi aktivasi fisika pada pembuatan karbon aktif dari limbah tempurung kelapa', (Review: Physical activation technology in the manufacture of activated carbon from coconut shell waste), *Jurnal Teknik Kimia*, vol. 26, no. 2, pp. 42-53, https://doi.org/10.36706/jtk.v26i2.518

Rashidi, NA, Yusup, S, Borhan, A & Loong, LH 2014, 'Experimental and modelling studies of carbon dioxide adsorption by porous biomass derived activated carbon', *Clean Technologies and Environmental Policy*, vol. 16, pp. 1353-1361, https://doi.org/10.1007/s10098-014-0788-6

Rosyadi, AI, Harianto, S & Prawira-Atmaja, MI 2018, 'Karakteristik pelet kayu dari limbah pangkasan teh berdasarkan besaran partikel', (Characteristics of wood pellets from tea pruning waste based on particle size), *Jurnal Penelitian Teh dan Kina*, vol. 21, pp. 18-25

Sudibandriyo, M & Rizki, A 2024, 'The influence of activated carbon as adsorbent in adsorptive–distillation of ethanol–water mixture', *International Journal of Technology*, vol. 15, no. 2, pp. 425-431, https://doi.org/10.14716/ijtech.v15i2.6659

Sun, Y & Webley, PA 2010, 'Preparation of activated carbons from corncob with large specific surface area by a variety of chemical activators and their application in gas storage', *Chemical Engineering Journal*, vol. 162, pp. 883-892, https://doi.org/10.1016/j.cej.2010.06.031

Tabak, A, Sevimli, K, Kaya, M & Caglar, B 2019, 'Preparation and characterization of a novel activated carbon component via chemical activation of tea woody stem', *Journal of Thermal Analysis and Calorimetry*, vol. 138, pp. 3885-3895, https://doi.org/10.1007/s10973-019-08387-2

Titiladunayo, IF, Mcdonald, AG & Fapetu, OP 2012, 'Effect of temperature on biochar product yield from selected lignocellulosic biomass in a pyrolysis process', *Waste and Biomass Valorization*, vol. 3, pp. 311-318, https://doi.org/10.1007/s12649-012-9118-6

Wulansari, R & Rezamela, E 2020, 'Effect of black tea waste compost (tea fluff) on the growth of tea seedlings (*Camellia sinensis* (L.) Kuntze)', *Journal of Soil and Land Resources*, vol. 7, pp. 341-350, https://doi.org/10.21776/ub.jtsl.2020.007.2.19

Yek, PNY, Liew, RK, Osman, MS, Lee, CL, Chuah, JH, Park, YK & Lam, SS 2019, 'Microwave steam activation, an innovative pyrolysis approach to convert waste palm shell into highly microporous activated carbon', *Journal of Environmental Management*, vol. 236, pp. 245-253, https://doi.org/10.1016/j.jenvman.2019.01.010

Yıldız, Z, Kaya, N, Topcu, Y & Uzun, H 2019, 'Pyrolysis and optimization of chicken manure wastes in fluidized bed reactor: CO₂ capture in activated bio-chars', *Process Safety and Environmental Protection*, vol. 130, pp. 297-305, https://doi.org/10.1016/j.psep.2019.08.011

Yuliusman, Purwanto, WW & Nugroho, YS 2015, 'Smoke clearing method using activated carbon and natural zeolite', *International Journal of Technology*, vol. 6, no. 3, pp. 492-503, https://doi.org/10.14716/ijtech.v6i3.1125

Yuliusman, Putri, SA, Sipangkar, SP, Al Farouq, F & Fatkhurrahman, M 2019, 'Technology development of adsorption cigarette smoke using modified activated carbon with MgO from waste biomass of durian shell', *International Journal of Technology*, vol. 10, no. 8, pp. 1505-1512, https://doi.org/10.14716/ijtech.v10i8.3489

Zhou, J, Luo, A & Zhao, Y 2018, 'Preparation and characterisation of activated carbon from waste tea by physical activation using steam', *Journal of the Air & Waste Management Association*, vol. 68, pp. 1269-1277, https://doi.org/10.1080/10962247.2018.1460282

Zubbri, NA, Mohamed, AR, Lahijani, P & Mohammadi, M 2021, 'Low temperature CO₂ capture on biomass-derived KOH-activated hydrochar established through hydrothermal carbonization with water-soaking pre-treatment', *Journal of Environmental Chemical Engineering*, vol. 9, article 105074, https://doi.org/10.1016/j.jece.2021.105074